Reducing motion artifacts in diffusion-weighted MR images of the brain: Efficacy of navigator echo correction and pulse triggering

Olaf Dietrich, Sabine Heiland, Thomas Benner, Klaus Sartor

Department of Neuroradiology, University of Heidelberg Medical School, Heidelberg, Germany

Abstract

Diffusion-weighted magnetic resonance imaging (DWI) is extremely sensitive to motion of the examined object. Pulse triggering and navigator echo correction are methods to reduce motion artifacts that can be combined with conventional DWI sequences. Implementations of these methods in imaging sequences with a readout of one, three, or five spin echoes are presented and imaging results are compared in a study with five healthy volunteers. As an objective measure for motion-induced image artifacts, the *artifacticity* of an image is defined. It is shown that pulse triggering and navigator echo correction significantly improve image quality and hence provide a technique for high quality DWI on standard scanners without improved gradient hardware.

Keywords

Diffusion-weighted magnetic resonance imaging, Motion artifacts, Navigator echo correction, Pulse triggering

Correspondence to

Olaf Dietrich
Department of Neuroradiology
University of Heidelberg Medical School
Im Neuenheimer Feld 400
D-69120 Heidelberg, Germany
E-mail: olaf.dietrich@urz.uni-heidelberg.de
Telephone: +49–6221–567566
Fax: +49–6221–564673

Introduction

Diffusion-weighted magnetic resonance imaging (DWI) of the brain has been shown to be of great value in early detection of cerebral ischemia [1, 2, 3, 4, 5] and in therapy monitoring of stroke patients [6, 7, 8]. Other clinical applications, such as white matter fiber tract imaging by determining diffusion anisotropy [9, 10, 11, 12], or experimental applications such as determining cell size [13, 14, 15] and tissue temperature mapping [16, 17] contribute to the importance of this technique. DWI is based on the effects of the microscopic brownian motion (diffusion) of water molecules in tissue. In addition to ρ-, T_1-, or T_2-contrast, the strength of water diffusion influences directly the image intensity in the resulting diffusion-weighted images.

Magnetic resonance (MR) imaging sequences can be diffusion-sensitized by adding a pair of strong gradients according to the Stejskal-Tanner scheme [18]. These gradients cause phase changes of the proton spins proportional to their stochastic spatial displacement and hence an intensity attenuation in the reconstructed image directly depending on the local diffusion coefficient. The quantitative dependence between diffusion constant D and image intensity I is described by the so-called b-value, a parameter that is dependent on strength and timing (duration δ and separation of onsets Δ) of the diffusion gradients (gyromagnetic ratio γ, gradient strength G) [18]:

$$\ln \frac{I(b)}{I_0} = -bD = -(\gamma G\delta)^2(\Delta - \frac{\delta}{3})D. \qquad (1)$$

The apparent diffusion coefficient (ADC) can be calculated from two or more diffusion-weighted images with different b-values; it is called *apparent* because it results from a mixture of intra- and extracellular diffusion coefficients and systematic shifts due to restricted diffusion [14, 19, 20] effects. The Stejskal-Tanner gradient scheme is widely used because it can be combined with different imaging techniques ranging from simple spin echo (SE) to echo planar imaging (EPI) [21, 22, 23].

An important limitation to the application of DWI in clinical routine is the frequently observed severe image degradation caused by involuntary patient motion. The two main components of motion in brain imaging are bulk motion (translation and rotation) of the whole head and the periodic local motion of brain tissue due to cerebral spinal fluid pulsation. As a consequence of the sensitivity of DWI to microscopic stochastic motion in the micrometer range, this method is extremely susceptible to macroscopic motion of the imaged object as well. Already tissue motion in the submillimeter range during the diffusion-weighting period already leads to severe image artifacts. Different approaches have been suggested to overcome motion-induced image artifacts [24], including multiple image averaging [25], radial projection reconstruction [26], use of less bulk-motion sensitive sequences (e. g. by using velocity-compensating gradients [27]), single-shot imaging methods such as high-speed STEAM [28], GRASE [29], or EPI [21, 22, 23], pulse triggering or cardiac gating [30], and the correction of acquired data using navigator echoes. Navigator echoes are additionally acquired echoes with constant phase encoding which differ from each other only due to motion-induced phase shifts [31, 32]. Thus, these phase shifts can be calculated and applied inversely to the corresponding image raw data to remove the effects of bulk motion and hence motion artifacts. Several studies showed qualitatively the benefit of navigator echo (NAV) correction applied to DWI [33, 34, 35].

The objective of our study was to evaluate quantitatively the efficacy of NAV correction and of pulse triggering in DWI. Both methods were compared when used separately or combined. Their efficacy was evaluated with three different imaging sequences under additional consideration of acquisition time and image quality.

Methods

Sequences: A conventional SE sequence and two sequences with multiple spin echo readout (MSE) were implemented on a clinical 1.5 T MR scanner (Edge, Picker, Cleveland, Ohio, USA) with standard hardware (maximum gradient strength 15 mT/m, minimum rise time 750 μs). All sequences were extended with Stejskal-Tanner diffusion gradients and an additional navigator echo readout at constant (zero) phase encoding. The MSE sequences contained a series of 180° radio frequency pulses to acquire either 3 (MSE 3) or 5 (MSE 5) spin echoes after each excitation, which were used as image data. Hence, the total number of acquired echoes after each excitation including the navigator echo was 2 (SE), 4, and 6 (MSE). The general sequence parameters are summarized in Table 1 and a sequence scheme showing the position of

the navigator readout is given in Figure 1. The acquisition timing of all sequences could be synchronized with the pulse as measured by a finger pulse sensor (photoplethysmograph).

Postprocessing: The aim of our study was to quantify the strength of motion artifacts in diffusion-weighted images depending on the use of navigator echo correction and pulse triggering with different sequences. Therefore, an objective measure of amount and severity of artifacts had to be established. Basically, the quotient of mean image intensity outside the imaged object and within the imaged object was defined as the *artifacticity* A of the image, but because of the typical form of motion artifacts in DWI a slightly more complicated algorithm had to be used.

Determining the mean intensity I_0 within the imaged object is difficult because motion artifacts result in image intensity spread all over the field of view (FOV) mainly in phase-encoding direction. Hence, image intensity cannot be defined as the intensity in a certain image region, but was redefined to be the mean value of the intensities of the brightest 30 % of all image pixels, which however were not necessarily found in the original area of the imaged object. The empirically determined fraction of 30 % of all pixels is sufficiently large to include a main portion of intense tissue, but it does not contain any background area in the acquired slices. The corresponding intensity limit $I_{70\,\%}$ can be calculated from the integral $H(I)$ of the intensity histogram function $h(I)$ of the image:

$$H(I) = \int_0^I \mathrm{d}I'\, h(I'). \tag{2}$$

Let $N = H(I_{\max})$ be the total number of pixels (with $I_{\max}$ the maximum pixel intensity in the image), then, using the inverse function H^{-1}, the intensity limit to a given fraction f of all pixels is given by

$$I_f = H^{-1}(fN). \tag{3}$$

E. g. $I_{70\,\%} = H^{-1}(0.7\,N)$ is the intensity limit such that 70 % of all image pixels are less intense than $I_{70\,\%}$. The exact formula for the *mean intensity of the imaged object* is:

$$I_0 = \int_{I_{70\,\%}}^{I_{98\,\%}} \mathrm{d}I'\, I' h(I') \Bigg/ \int_{I_{70\,\%}}^{I_{98\,\%}} \mathrm{d}I'\, h(I')\ . \tag{4}$$

The brightest 2 % of all image pixels were not taken into account to avoid bias by solitary intensity peaks due to reconstruction artifacts.

To determine the mean intensity I_M outside the original image area, which is caused by motion during the acquisition, an elliptic mask was manually defined as shown in Figure 2. Definition of the mask was done on a maximum intensity projection of all slices of the images acquired without diffusion-weighting ($b = 0$) and hence without severe motion artifacts. The intensity I_N of statistical noise was subtracted from I_M to determine motion-induced artifact intensity only. To calculate the noise intensity I_N, two horizontal background areas were defined in the oversampling region adjacent to the normal image as shown in Figure 2c; these regions above and below the imaged object were not affected by motion artifacts. Image masks were defined separately for each individual. Finally, the artifacticity A was defined as:

$$A = \frac{I_M - I_N}{I_0}. \tag{5}$$

The same quantities were used to define the signal-to-noise ratio (SNR) of diffusion-weighted images:

$$R_{SN} = \frac{I_0}{I_N}. \tag{6}$$

The results agree with the conventional definition of the SNR for average images. However, the particular form of the signal definition (I_0) leads to a SNR of about 1.7 for images containing only white noise; thus, a systematic shift of the SNR for very noisy images is to be expected.

Patient examination: The study included 5 healthy volunteers (4 male, 1 female, age 25 y to 31 y, ⌀ : 27 y). All sequences (SE, MSE 3, MSE 5) with navigator echo readout were applied on all volunteers in three passes:

- with diffusion gradients in phase encoding direction [34] and b-value 550 s mm^{-2}; repetition time T_R = 1500 ms;
- with diffusion gradients in phase encoding direction and b-value 550 s mm^{-2}; acquisition was synchronized with pulse using the finger pulse sensor; T_R was set to 2 pulse cycles (about 1850 ms);
- without diffusion gradients ($b = 0$) and without pulse triggering; all other parameters were as above (T_R = 1500 ms).

Table 1: Acquisition parameters of sequences SE, MSE 3, and MSE 5. See Figure 1 for the definition of timing parameters.

Sequence		SE	MSE 3	MSE 5
Number of spin echo readouts		2	4	6
Number of image data readouts		1	3	5
Pseudo echo time	$\frac{T_{E1}}{ms}$	100.0	90.0	90.0
Echo time for navigator	$\frac{T_{E2}}{ms}$	126.0	105.0	105.0
Inter echo time	$\frac{T_{IE}}{ms}$	26.0	15.0	15.0
Image matrix (phase×readout)		159×192	162×192	160×200
Minimum FOV	$\frac{FOV}{mm}$	80	100	100
Minimum slice thickness	$\frac{d}{mm}$	1	5	5
Duration of diffusion gradients	$\frac{\delta}{ms}$	37.5	36.9	36.9
Diffusion time	$\frac{\Delta}{ms}$	45.4	45.0	45.0
Maximum *b*-value[a]	$\frac{b_{max}}{s\,mm^{-2}}$	664	623	655
Acquisition time[a] (T_R = 1500 ms)	$\frac{T_{acq}}{s}$	245	98	65
Acquisition time[a] (pulse triggering)	$\frac{T_{acq}}{s}$	309	117	85

[a] The maximum *b*-values and the acquisition times refer to a FOV of 220 mm, acquisition of 4 slices, and T_R = 1500 ms ($T_R \approx$ 1850 ms for pulse-triggered acquisition).

Four axial images (slice thickness 5 mm and slice distance 15 mm) above the orbito-meatal line were acquired; the rectangle FOV was about 220 mm × 176 mm, slightly varying with the matrix size (see Table 1). Acquisition times for 4 slices ranging from 65 s to 309 s are given in Table 1. Since "ideal" cooperation could be expected from the volunteers (compared to a typical patient population), they were asked to minimize head motion during the acquisition, but no head fixation or immobilization was applied.

After acquisition, the raw data were transferred to an external workstation (Aries Ultrastation 1 Model 170, Aries, Fremont, California, USA), where the NAV correction and data evaluation was performed by a self-written Matlab routine (MathWorks Inc., Natick, Massachusetts, USA). From each acquisition two sets of images were reconstructed: one using the additional motion information that could be extracted from the NAV readout and one discarding this information. These image sets were compared with each other and with the corresponding images from each of the three passes in order to evaluate the efficacy of motion correction. The NAV correction here implemented did not use any fit algorithm to calculate head translation [33] or rotation [34] but applied the complete phase information that was extracted from the navigator echoes to the image raw data.

Mean values of artifacticity and SNR were calculated by averaging over all slices and all volunteers; this was done separately for original and corrected images from each acquisition pass and each sequence.

Results

Figure 3 demonstrates the efficacy of motion artifact reduction in DWI with pulse triggering and the NAV approach in examples from all three sequences. Image quality improves distinctly with advancing stage of motion correction. Severe motion artifacts appear in the images without navigator correction (column 1 and 2) left and right from the imaged object as a consequence of bulk head motion and pulsatile brain motion (column 1). The latter causes an intensity loss particularly in the regions of the ventricles (e. g. image C1) and artifacts on both sides of the ventricles in the vertical center of the images. These vertically centered artifacts remain after navigator correction alone (images A3, C3), but occur to a much lower degree in slices above the ventricles (image B3). The benefit of pulse triggering cannot be observed in image C2 because of the presumably strong head motion in this case. Finally, after combined application of pulse triggering and NAV correction, arti-

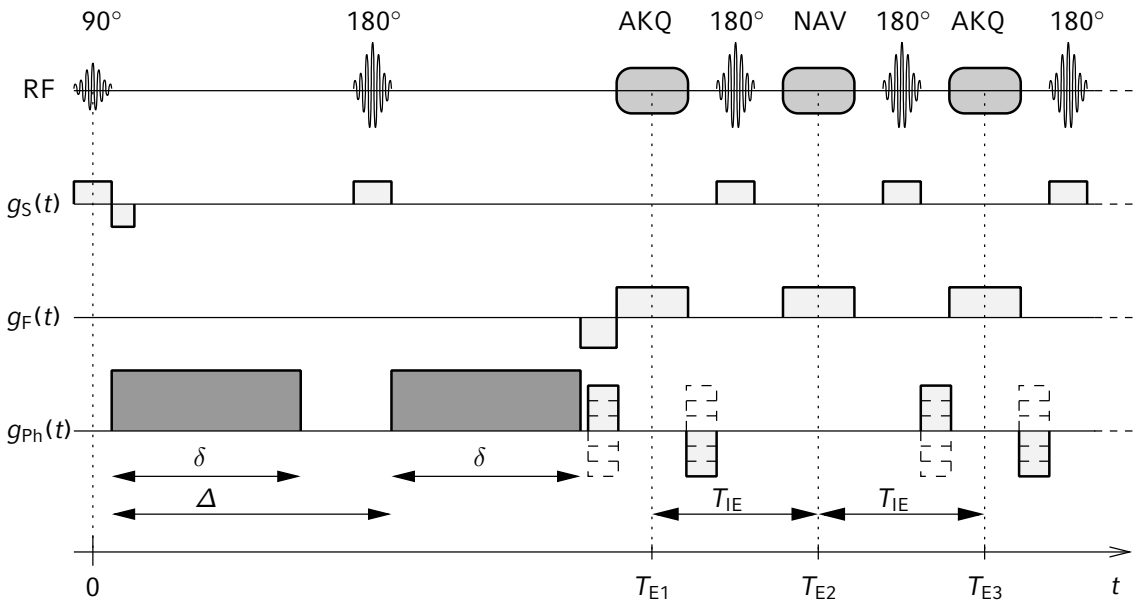

Figure 1: MSE sequence scheme. The total number of acquisition echoes (ACQ) after each excitation is either 3 or 5; the navigator echo (NAV) is inserted after the first ACQ. This scheme is also valid for the SE sequence: in this case it ends after the NAV. See Table 1 for sequence parameters.

facts almost completely disappear (column 4). The NAV correction worked evenly successfully and without problems independently of the individual differences in kind and strength of motion.

Comparison of the three fully motion-compensated sequences (column 4) shows a decreasing SNR and reduced image contrast from SE to MSE 5; however, the efficacy of motion artifact correction is similar. Calculated SNR values for pulse-triggered acquisitions are 12.3 ± 0.9 (SE), 8.5 ± 0.8 (MSE 3), and 8.1 ± 0.9 (MSE 5). The SNR for the three acquisition passes mentioned above is shown in Figure 4. Whereas a higher SNR is observed for acquisition without diffusion-weighting, there is no significant difference whether or not pulse triggering is used.

Quantitative results of artifacticity calculation are shown in Figure 5. The mean artifacticity A is about 0.14 ± 0.05 for uncorrected data and about 0.02 ± 0.01 for images after both pulse-triggered acquisition and navigator correction consistently for all three sequences. In detail, the artifacticity A is reduced by 91 % in SE images, 87 % in MSE 3 images, and 84 % in MSE 5 images comparing uncorrected and optimally corrected images.

Discussion

Navigator echo correction combined with pulse-triggered acquisition provides a robust and efficient method for DWI on MR scanners with conventional gradient hardware. A significant reduction of motion artifacts is achieved as was reported before for SE sequences with NAV correction [33, 34, 35]; in most cases no artifacts could be visually observed after the correction. The same holds true for imaging with an extended readout of multiple spin echoes that reduces acquisition time by a factor of about 3 to 4.

In detail, artifact reduction gains significantly more from NAV correction than from pulse triggering, which shows that bulk motion is generally predominant over pulsatile brain motion. In slices above the ventricles, pulsatile brain motion seems to be negligible in many cases. However, this depends on the direction of the diffusion gradients, which was in-plane in our study and thus perpendicular to the (radial) main component of pulsatile motion above the ventricles. Therefore, acquiring with NAV correction alone can be recommended if the slice position is above the ventricles. The finger sensor for pulse triggering can be easily applied, though, even after positioning the patient in the scanner and hence may be used always to minimize the influence of pulsatile motion as far as possible. The main disadvantage of pulse triggering is a prolongation of acquisition time depending on the pulse rate and regularity of the pulse; in this volunteer study, acquisition time was extended by 20 %–30 %, but a greater prolongation should be expected for a typical patient population.

All three examined sequences showed similar re-

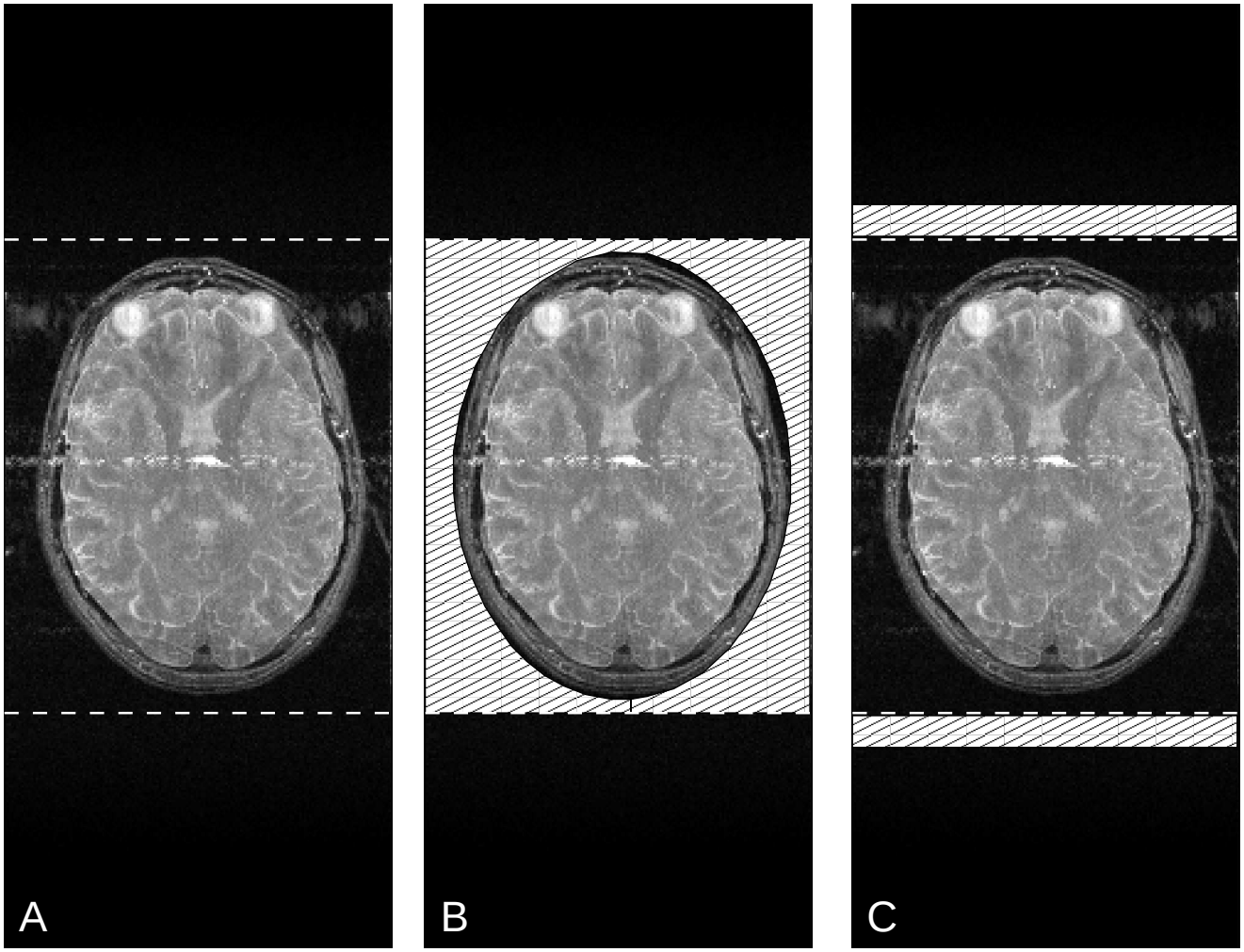

Figure 2: Image masks used for calculation of artifacticity. (A) Maximum intensity projection through 4 slices acquired without diffusion-weighting. The image is displayed with the oversampling area in readout direction separated by dashed lines. (B) The hatched region was used to calculate the intensity I_M of motion artifacts. (C) Regions for calculation of background noise I_N.

sults concerning motion sensitivity and correction. Whereas the efficacy of motion correction was identical, the image quality decreased with an increasing number of readout spin echoes and hence with decreasing acquisition time as a consequence of T_2-relaxation. This became apparent in visibly reduced tissue contrast and decreasing SNR. Geometrical distortions or local image artifacts were not observed. For routine use, the image quality of the fast MSE 5 sequence should prove to be sufficient. However, if very high image quality is desired and acquisition time is not a limiting factor, use of the SE sequence with navigator correction and pulse triggering is recommended because of its higher SNR. Sequences with more than 5 image echo readouts may be designed to accelerate the acquisition, but a lower SNR and worse image quality must be expected. Without faster gradients, the readout will be prolonged for such sequences, leading to stronger T_2-relaxation. The presented MSE 5 sequence appears to be a good compromise for the given gradient hardware.

Comparing these methods with diffusion-weighted single-shot EPI [23], which is the most frequently used alternative method for DWI, several arguments should be considered. The main advantages of single-shot EPI are the insensitivity to bulk motion and pulsatile brain motion and the very short acquisition time. Thus, image averaging can be performed without causing unreasonably long acquisition times, and different diffusion gradients can be applied either in one direction to use more than two b-values for ADC calculation or in different spatial directions to calculate diffusion tensor images [9]. On the other hand, EPI images are typically affected by susceptibility artifacts [36], eddy current artifacts [37], and hence, depending on slice position, gross geometrical distortions; this is especially disadvantageous if superposition on morphologic images is necessary. Another con-

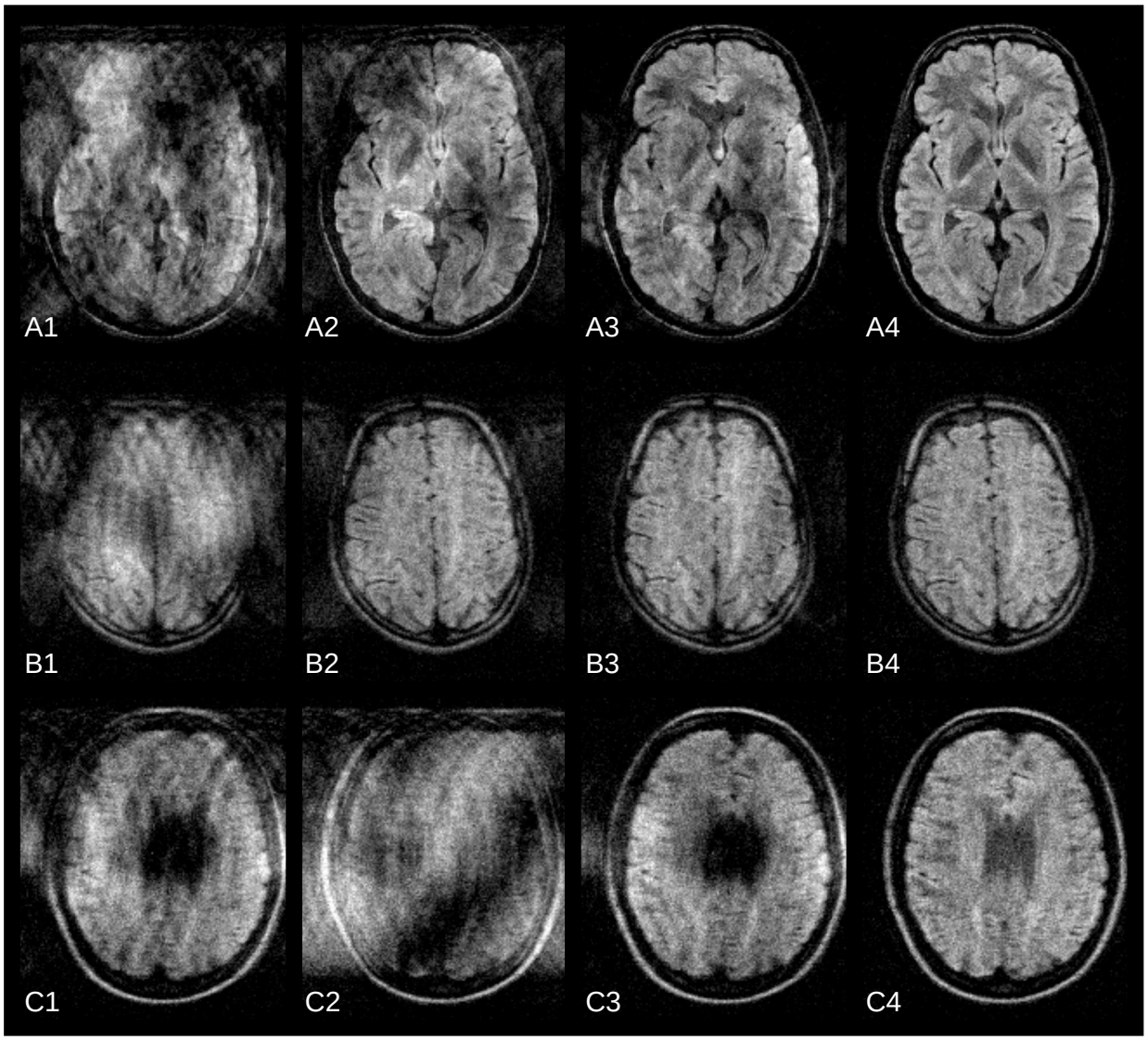

Figure 3: Examples for advancing stages of motion correction for all sequences (row A: SE, B: MSE 3, C: MSE 5). Column 1: non-corrected images, 2: acquisition with pulse triggering, 3: images after NAV correction, 4: combination of pulse triggering and NAV correction. To present a broad variety of results, images in each of the three rows are taken from different volunteers and different slice positions.

sequence of the relatively long EPI readout are inhomogeneous image contrasts due to T_2- and T_2^*-effects. Finally, single-shot EPI requires extended gradient facilities with strong and fast-switching gradients, that are not available on many scanners. Therefore, if either single-shot EPI cannot be performed due to hardware restrictions or if high image quality with minimized geometrical distortions is desired, the use of navigator-corrected, pulse-triggered MSE sequences is recommended.

To perform tensor imaging with a NAV-corrected sequence, it would be necessary to extend the sequence scheme. The presented sequences can correct for rotational phase shifts only with the diffusion gradient in phase direction [34]. For other diffusion directions, the navigator echo should be acquired not only in readout direction but also in phase direction, requiring then a much more complicated correction algorithm; otherwise, only the translational component of bulk motion can be corrected. Because of the resulting long acquisition time for tensor imaging without single-shot sequences, this approach was not further investigated in this study.

Multiple signal averaging as another method to suppress motion artifacts requires a much longer acquisition time depending on the number of averages (usually between 4 and 16 [25]), whereas the navigator readout can be added without significant prolongation of acquisition. While the use of flow-compensated gradients has the disadvantage (similar to most single-shot methods) that an advanced gradient system is needed, the NAV correction contents itself with standard imaging

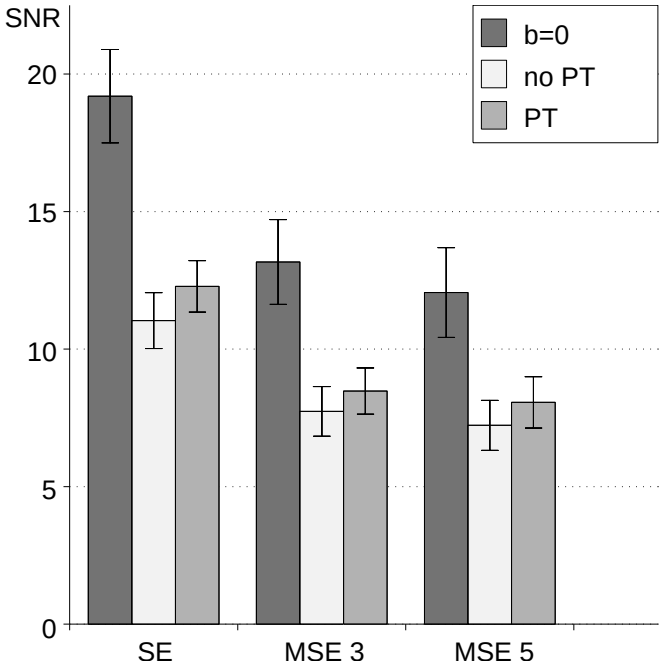

Figure 4: SNR for different sequences (SE, MSE 3, MSE 5) without diffusion weighting (b = 0), with diffusion weighting but without pulse triggering (no PT), and with both diffusion weighting and pulse triggering (PT).

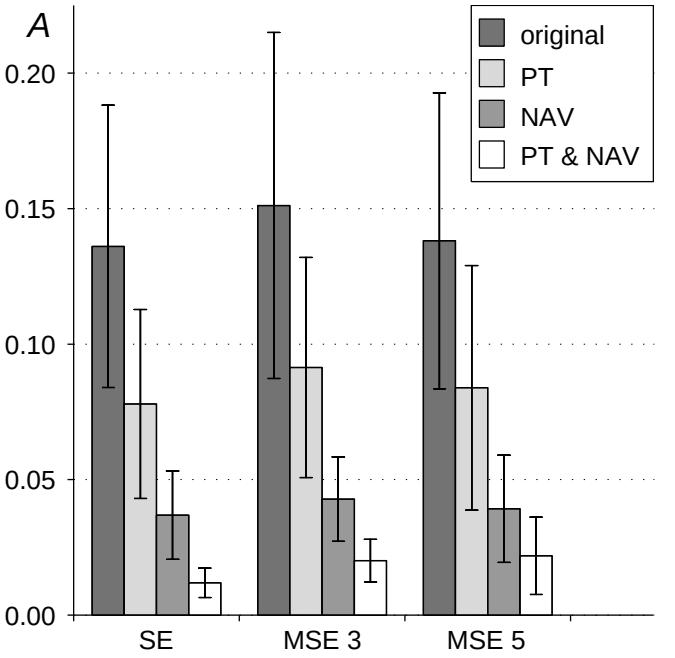

Figure 5: Artifacticity A for different stages of motion correction (PT: pulse triggering, NAV: navigator correction) and three different sequences (SE, MSE 3, MSE 5).

gradients.

In conclusion, we were able to show that DWI can be performed in good image quality on scanners with conventional gradient hardware if both NAV correction and pulse triggering are used. Longer acquisition times than for single-shot EPI sequences must be accepted, but are rewarded by higher image quality. Motion artifacts are not inevitable in DWI without EPI hardware.

References

1. Moseley ME, Cohen Y, Mintorovitch J, Chileuitt L, Shimizu H, Kucharczyk J, Wendland MF, Weinstein PR (1990) Early detection of regional cerebral ischemia in cats: comparison of diffusion- and T2-weighted MRI and spectroscopy. Magn. Reson. Med. 14: 330–346

2. Moseley ME, Kucharczyk J, Mintorovitch J, Cohen Y, Kurhanewicz J, Derugin N, Asgari H, Norman D (1990) Diffusion-weighted MR imaging of acute stroke: correlation with T2-weighted and magnetic susceptibility-enhanced MR imaging in cats. AJNR Am. J. Neuroradiol. 11: 423–429

3. Lövblad KO, Baird AE, Schlaug G, Benfield A, Siewert B, Voetsch B, Connor A, Burzynski C, Edelman RR, Warach S (1997) Ischemic lesion volumes in acute stroke by diffusion-weighted magnetic resonance imaging correlate with clinical outcome. Ann. Neurol. 42: 164–170

4. Tong DC, Yenari MA, Albers GW, O'Brien M, Marks MP, Moseley ME (1998) Correlation of perfusion- and diffusion-weighted MRI with NIHSS score in acute (<6.5 hour) ischemic stroke. Neurology 50: 864–870

5. Singer MB, Chong J, Lu D, Schonewille WJ, Tuhrim S, Atlas SW (1998) Diffusion-weighted MRI in acute subcortical infarction. Stroke 29: 133–136

6. Fischer M, Bockhorst K, Hoehn-Berlage M, Schmitz B, Hossmann KA (1995) Imaging of the apparent diffusion coefficient for the evaluation of cerebral metabolic recovery after cardiac arrest. Magn. Reson. Imaging 13: 781–790

7. Tarr RW (1997) Brain attack. Clinical monitoring of early pathophysiologic events. Neurosurg. Clin. N. Am. 8: 179–194

8. Hossmann KA, Hoehn-Berlage M (1995) Diffusion and perfusion MR imaging of cerebral ischemia. Cerebrovasc. Brain. Metab. Rev. 7: 187–217

9. Douek P, Turner R, Pekar J, Patronas N, Le Bihan D (1991) MR color mapping of myelin fiber orientation. J. Comput. Assist. Tomogr. 15: 923–929

10. Brunberg JA, Chenevert TL, McKeever PE, Ross DA, Junck LR, Muraszko KM, Dauser R, Pipe JG, Betley AT (1995) In vivo MR determination of water diffusion coefficients and diffusion anisotropy: correlation with structural alteration in gliomas of the cerebral hemispheres. AJNR Am. J. Neuroradiol. 16: 361–371

11. Pierpaoli C, Jezzard P, Basser PJ, Barnett A, Di Chiro G (1996) Diffusion tensor MR imaging of the human brain. Radiology 201: 637–648

12. Buchsbaum MS, Tang CY, Peled S, Gudbjartsson H, Lu D, Hazlett EA, Downhill J, Haznedar M, Fallon JH, Atlas SW (1998) MRI white matter diffusion anisotropy and PET metabolic rate in schizophrenia. Neuroreport 9: 425–430

13. Anderson AW, Zhong J, Petroff OA, Szafer A, Ransom BR, Prichard JW, Gore JC (1996) Effects of osmotically driven cell volume changes on diffusion-weighted imaging of the rat optic nerve. Magn. Reson. Med. 35: 162–167

14. Pilatus U, Shim H, Artemov D, Davis D, van Zijl PC, Glickson JD (1997) Intracellular volume and apparent diffusion constants of perfused cancer cell cultures, as measured by NMR. Magn. Reson. Med. 37: 825–832

15. Kuchel PW, Coy A, Stilbs P (1997) NMR "diffusion-diffraction" of water revealing alignment of erythrocytes in a magnetic field and their dimensions and membrane transport characteristics. Magn. Reson. Med. 37: 637–643

16. Bleier AR, Jolesz FA, Cohen MS, Weisskoff RM, Dalcanton JJ, Higuchi N, Feinberg DA, Rosen BR, McKinstry RC, Hushek SG (1991) Real-time magnetic resonance imaging of laser heat deposition in tissue. Magn. Reson. Med. 21: 132–137

17. MacFall J, Prescott DM, Fullar E, Samulski TV (1995) Temperature dependence of canine brain tissue diffusion coefficient measured in vivo with magnetic resonance echo-planar imaging. Int. J. Hyperthermia 11: 73–86

18. Stejskal OE, Tanner JE (1965) Spin diffusion measurements: spin echoes in the presence of a time-dependent field gradient. J. Chem. Phys. 42: 288–292

19. Norris DG, Niendorf T, Hoehn-Berlage M, Kohno K, Schneider EJ, Hainz P, Hropot M, Leibfritz D (1994) Incidence of apparent restricted diffusion in three different models of cerebral infarction. Magn. Reson. Imaging 12: 1175–1182

20. Stanisz GJ, Szafer A, Wright GA, Henkelman RM (1997) An analytical model of restricted diffusion in bovine optic nerve. Magn. Reson. Med. 37: 103–111

21. Turner R, Le Bihan D, Maier J, Vavrek R, Hedges LK, Pekar J (1990) Echo-planar imaging of intravoxel incoherent motion. Radiology 177: 407–414

22. Stehling MK, Turner R, Mansfield P (1991) Echo-planar imaging: magnetic resonance imaging in a fraction of a second. Science 254: 43–50

23. Turner R, Le Bihan D, Chesnick AS (1991) Echo-planar imaging of diffusion and perfusion. Magn. Reson. Med. 19: 247–253

24. Trouard TP, Sabharwal Y, Altbach MI, Gmitro AF (1996) Analysis and comparison of motion-correction techniques in diffusion-weighted imaging. J. Magn. Reson. Imaging 6: 925–935

25. Merboldt KD, Hänicke W, Gyngell ML, Frahm J, Bruhn H (1989) The influence of flow and motion in MRI of diffusion using a modified CE-FAST sequence. Magn. Reson. Med. 12: 198–208

26. Gmitro AF, Alexander AL (1993) Use of a projection reconstruction method to decrease motion sensitivity in diffusion-weighted MRI. Magn. Reson. Med. 29: 835–838

27. Brockstedt S, Thomsen C, Wirestam R, De Poorter J, De Wagter C, Salford LG, Holtås S, Stahlberg F (1995) Use of an enhanced gradient system for diffusion MR imaging with motion-artifact reduction. Acta. Radiol. 36: 662–670

28. Merboldt KD, Hänicke W, Bruhn H, Gyngell ML, Frahm J (1992) Diffusion imaging of the human brain in vivo using high-speed STEAM MRI. Magn. Reson. Med. 23: 179–192

29. Johnson G, Feinberg DA, Venkataraman V (1996) Single-shot GRASE imaging with short effective TEs. J. Magn. Reson. Imaging 6: 944–947

30. Posse S, Cuenod CA, Le Bihan D (1993) Human brain: proton diffusion MR spectroscopy. Radiology 188: 719–725

31. Ehman RL, Felmlee JP (1989) Adaptive technique for high-definition MR imaging of moving structures. Radiology 173: 255–263

32. Korin HW, Felmlee JP, Ehman RL, Riederer SJ (1990) Adaptive technique for three-dimensional MR imaging of moving structures. Radiology 177: 217–221

33. Ordidge RJ, Helpern JA, Qing ZX, Knight RA, Nagesh V (1994) Correction of motional artifacts in diffusion-weighted MR images using navigator echoes. Magn. Reson. Imaging 12: 455–460

34. Anderson AW, Gore JC (1994) Analysis and correction of motion artifacts in diffusion weighted imaging. Magn. Reson. Med. 32: 379–387

35. de Crespigny AJ, Marks MP, Enzmann DR, Moseley ME (1995) Navigated diffusion imaging of normal and ischemic human brain. Magn. Reson. Med. 33: 720–728

36. Lövblad KO, Jakob PM, Chen Q, Baird AE, Schlaug G, Warach S, Edelman RR (1998) Turbo spin-echo diffusion-weighted MR of ischemic stroke. AJNR Am. J. Neuroradiol. 19: 201–208

37. Alexander AL, Tsuruda JS, Parker DL (1997) Elimination of eddy current artifacts in diffusion-weighted echo-planar images: the use of bipolar gradients. Magn. Reson. Med. 38: 1016–1021